

**Abstract.** We have developed a high-precision code which solves the kinematic dynamo problem both for given rotation law and meridional flow in the case of a low eddy diffusivity of the order of  $10^{11} \text{ cm}^2/\text{s}$  known from the sunspot decay. All our models work with an  $\alpha$ -effect which is positive (negative) in the northern (southern) hemisphere. It is concentrated in radial layers located either at the top or at the bottom of the convection zone. We have also considered an  $\alpha$ -effect uniformly distributed in all the convection zone. In the present paper the main attention is focused on i) the parity of the solution, ii) the form of the butterfly diagram and iii) the phase relation of the resulting field components. If the helioseismologically derived internal solar rotation law is considered, a model without meridional flow of high magnetic Reynolds number (corresponding to low eddy diffusivity) fails in all the three issues in comparison with the observations. However, a meridional flow with equatorial drift at the bottom of the convection zone of few meters by second can indeed enforce the equatorward migration of the toroidal magnetic field belts similar to the observed butterfly diagram but, the solution has only a dipolar parity if the (positive)  $\alpha$ -effect is located at the base of the convection zone rather than at the top. We can, therefore, confirm the main results of a similar study by Dikpati & Gilman (2001).

**Key words:** magnetohydrodynamics – Sun: interior – Sun: magnetic field

# Parity properties of an advection-dominated solar $\alpha^2 \Omega$ -dynamo

**A. Bonanno<sup>1</sup>, D. Elstner<sup>2</sup>, G. Rüdiger<sup>2</sup>, and G. Belvedere<sup>3</sup>**

<sup>1</sup> Osservatorio Astrofisico di Catania, Via S.Sofia 78, I-95123 Catania, Italy

<sup>2</sup> Astrophysikalisches Institut Potsdam, An der Sternwarte 16, D-14482 Potsdam, Germany

<sup>3</sup> Dipartimento di Fisica ed Astronomia, Via S.Sofia 78, I-95123, Catania, Italy

February 7, 2020

## 1. Introduction

In an early paper Roberts (1972) discussed the excitation conditions of distributed shell dynamos. The  $\alpha$ -effect, antisymmetric with respect to the equator, was considered in an outer shell ( $x_i \leq x \leq 1$ ,  $x = r/R_\odot$ ), the dynamo was embedded in vacuum and the differential rotation  $d\Omega/dx$  was considered as uniform throughout the outer shell. He found for positive dynamo numbers ( $\alpha_{\text{north}} \cdot d\Omega/dx > 0$ ) that dipoles are more easily excited than quadrupoles for thin convection zones whilst for deeper zones the quadrupoles are more easily excited (see Fig. 1).

These models are rather rough. The differences between the dipolar solutions and the quadrupolar solutions always happen to be small, so that the important question concerning the latitudinal symmetry, that is the parity, did not seem to be a serious problem.

Roberts & Stix (1972) computed  $\alpha^2 \Omega$ -dynamos with a rotation law similar to the solar rotation law known nowadays by helioseismology. The results are given in their Fig. 4b. Without latitudinal differential rotation ( $\beta = 0$ ) but with  $\partial\Omega/\partial x|_{\text{eq}} > 0$  the solution with quadrupolar (symmetric) parity has a lower eigenvalue than the solution with the dipolar symmetry (opposite to the Steenbeck-Krause (1969) model with  $\partial\Omega/\partial x|_{\text{eq}} < 0$ , see Fig. 3 of Roberts & Stix). The inclusion of the latitudinal shear produces still higher dynamo numbers but the difference between quadrupolar parity and dipolar parity grows.

Köhler (1973) thus considered only the excitation of modes with prescribed dipolar parity. For positive  $\alpha$ -effect in the northern hemisphere and with an outwards increasing  $\Omega$ , only a poleward drift of the toroidal magnetic field belts was found, contrary to the observations.

Moss & Brooke (2000), in order to produce the observed equatorward migration of the toroidal fields adopt the solar rotation law and a negative northern  $\alpha$ -effect in the bulk of the convection zone. The dipolar solutions are only slightly easier to excite than the quadrupolar ones (dipole:  $C_\alpha = -3.20$ , quadrupole  $C_\alpha = -3.25$ ). The parity problem does not seem to exist for negative dynamo numbers (see also Fig. 3 in Roberts & Stix 1972). The situation, however, completely changes if a

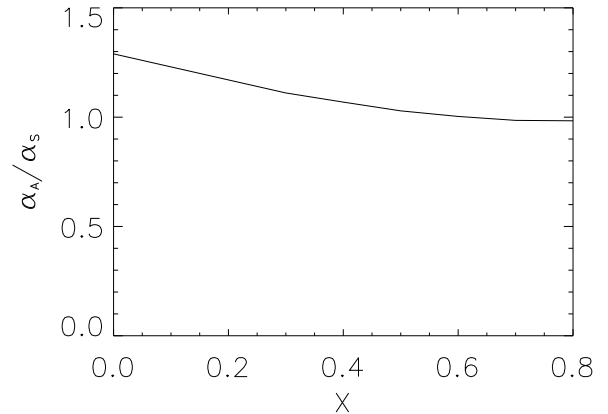


**Fig. 1.** The ratio of the dynamo numbers for equatorially antisymmetric (dipoles) to equatorially symmetric (quadrupoles) solutions for the shell dynamo of Roberts (1972). At  $x_i = 0.65$  both values are equal. For thinner shells the most efficient dynamo is of dipolar type while for thicker shells is of quadrupolar type.

positive northern  $\alpha$ -effect is considered (Roberts & Stix 1972, Fig. 4; Moss 1999). In this case one has to deal with a parity problem for the solar dynamo.

Following Dikpati & Gilman (2001) we shall here study the parity problem for solar dynamos in particular for dynamos with rather small eddy diffusivities so that the meridional flow plays an important role in advecting the toroidal magnetic field belts (Wang et al. 1991; Choudhuri et al. 1995). As the rotation law can be considered as given (known from helioseismology), we are free to vary the location of the  $\alpha$ -effect, so that models are assumed to have a positive  $\alpha$ -effect both at the top and at the bottom of the convection zone, as well as in the full convection zone.

The inclusion of the meridional flow  $u_m$  has a strong impact on the mean-field dynamo when the eddy diffusivity  $\eta_T$  is low. In particular, for  $\eta_T = 10^{11} \text{ cm}^2/\text{s}$ , as is known from the sunspot decay, the magnetic Reynolds number  $R_m = u_m R_\odot / \eta_T$  reaches values of the order of  $10^3$  for a flow of

10 m/s. As a consequence, depending on the localization of the dynamo wave, a dramatic modification of both magnetic field configurations and cycle period is expected. This possibility has recently been a subject of intense numerical investigation (Dikpati & Charbonneau 1999; Küker et al. 2001), where it has been shown that solutions with high magnetic Reynolds number provide correct cycle period, butterfly diagrams, magnetic phase relations and sign of current helicity, by means of a *positive*  $\alpha$ -effect in the north hemisphere.

In this investigation we study how the presence of the flow and the location of the turbulent layer affect the parity mode selection and the cycle period. In this respect we show that, for high magnetic Reynolds numbers of the flow, quadrupolar field configurations are more easily excited than the dipolar ones if there is no  $\alpha$ -effect below  $r/R_\odot \approx 0.8$ .

## 2. Basic equations

In the following the dynamo equations are given with the inclusion of the induction by meridional circulation. Axisymmetry implies that the mean flow in spherical coordinates is given by  $\mathbf{u} = (u_r, u_\theta, r \sin \theta \Omega)$ . (1)

In our formalism the magnetic field reads

$$\mathbf{B} = \left( \frac{1}{r \sin \theta} \frac{\partial A \sin \theta}{\partial \theta}, -\frac{1}{r} \frac{\partial A r}{\partial r}, B \right), \quad (2)$$

where  $A$  is the poloidal-field potential and  $B$  is the toroidal field. The dynamo equation may be written in the form  $\frac{\partial \mathbf{B}}{\partial t} = \text{rot}(\mathbf{u} \times \mathbf{B} + \alpha \mathbf{B}) - \text{rot}(\sqrt{\eta_T} (\text{rot} \sqrt{\eta_T} \mathbf{B}))$ , (3) which includes the diamagnetism due to non-uniform turbulence. In fact it has been shown (Kitchatinov & Rüdiger, 1992) that the diffusive part of the mean turbulent electromotive force reads  $-\eta_T \text{rot} \mathbf{B} - \nabla \eta_T \times \mathbf{B} / 2 = -\sqrt{\eta_T} \text{rot} \sqrt{\eta_T} \mathbf{B}$ . The second term is due to the turbulent diamagnetism. If there are strong gradients of turbulence intensity, this term will dominate the transport of the mean magnetic fields.

As usual, the meridional circulation is derived from a stream function, so that the condition  $\text{div} \rho \mathbf{u} = 0$  is automatically fulfilled. Then a series expansion in Legendre polynomials is introduced, as described in Rüdiger (1989):

$$\hat{u}_r = \frac{1}{r^2 \hat{\rho} \sin \theta} \frac{\partial \psi}{\partial \theta} = \sum_{2,4} \frac{1}{\hat{\rho} r^2} n(n+1) \Psi_n P_n, \quad (4)$$

$$\hat{u}_\theta = -\frac{1}{r \hat{\rho} \sin \theta} \frac{\partial \psi}{\partial r} = -\sum_{2,4} \frac{1}{\hat{\rho} r} \frac{d \Psi_n}{dr} P_n^{(1)}. \quad (5)$$

A one-cell meridional circulation is described by

$$u_r = \frac{3 \cos^2 \theta - 1}{\hat{\rho} x^2} \psi, \quad (6)$$

$$u_\theta = -\frac{\cos \theta \sin \theta}{\hat{\rho} x} \frac{d \psi}{dx}, \quad (7)$$

where  $\psi$  is the usual stream function. A positive  $\psi$  describes a cell circulating clockwise in the northern hemisphere, i.e. the flow is polewards at the bottom of the convection zone and equatorwards at the surface. For a negative  $\psi$  the flow is, as is observed, polewards at the surface. In order to keep the flow inside the convection zone, the function  $\psi$  must be zero at the

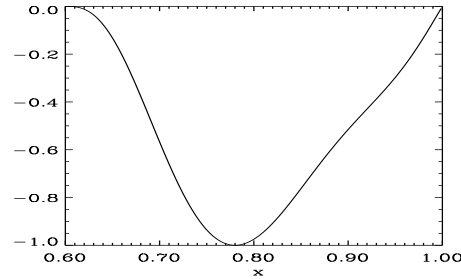


**Fig. 2.** The stream function  $\psi$  of the meridional circulation used in the model computations. It must be negative if the circulation shall proceed equatorwards at the surface.

surface and at the bottom of the convection zone. In order to define the strength of the flow, we shall use the values  $u_m$  of the meridional circulation at the bottom of the convection zone. The rotation law for the solar dynamo can be considered as given by the helioseismic observations, in particular we have used the analytical model of Dikpati & Charbonneau (1999) which is characterized by the existence of a steep subrotation profile in the polar region with a thickness of about 0.05 solar radii (see Markiel & Thomas 1999). We then define the profile of  $\eta_T$  as

$$\eta_T = \eta_c + \frac{1}{2} (\eta_t - \eta_c) (1 + \text{erf}(40(x - 0.7))), \quad (8)$$

where  $x = r/R_\odot$  is the fractional radius,  $\text{erf}$  denotes the error function,  $\eta_t$  is the eddy diffusivity, and  $\eta_c$  the magnetic diffusivity beneath the convection zone. The factor 40 defines the thickness of the transition region to be  $0.05R_\odot$ , and we have adopted both  $\eta_c/\eta_t = 0.1$  and  $\eta_c/\eta_t = 0.02$ .

There is an increasing evidence for an  $\alpha$ -effect in the convection zone rather than in the overshoot region. Observations of the turbulent current helicity by Seehafer (1990), Pevtsov et al. (1995), Abramenko et al. (1996) as well as Bao & Zhang (1998) always lead to *negative* values in the northern hemisphere and positive values in the southern hemisphere. If the observations indeed concern the current helicity of the *fluctuations* then after Rädler & Seehafer (1990) the azimuthal  $\alpha$ -effect should be *positive*. Also Brandenburg (1999) with new numerical simulations found (highly noisy) positive correlations between the turbulent EMF and the mean magnetic field, i.e. positive  $\alpha$ -effect for the northern hemisphere. Our SOCA theory of Lorentz force-driven turbulence in a stratified rotating plasma also leads to negative current helicity and positive  $\alpha$ -effect for the northern hemisphere (Rüdiger et al. 2001). Lastly, with their high-detailed simulation, Ossendrijver et al. (2001) show that indeed far beyond the limits of the SOCA theory the results are confirmed: in the northern part of the solar convection zone the horizontal  $\alpha$ -effect proves to be positive at variance with the vertical  $\alpha$ -effect and the current helicity.

The  $\alpha$ -effect is always antisymmetric with respect to the equator, so that we write

$$\alpha = \alpha_0 \cos \theta \left( 1 + \text{erf} \left( \frac{x - x_\alpha}{d} \right) \right) \left( 1 - \text{erf} \left( \frac{x - x_\beta}{d} \right) \right) / 4, \quad (9)$$

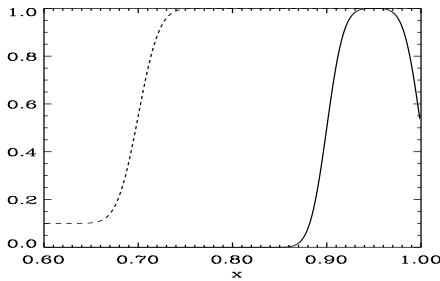


**Fig. 3.** The  $\alpha$ -effect normalized function in the bulk of the convection zone (solid line) and the profile of the eddy diffusivity (dashed line).

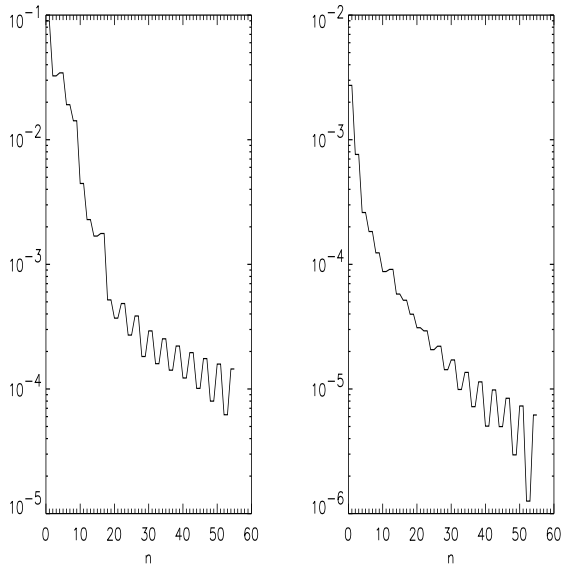


**Fig. 4.** Truncation dependence of a typical high-Reynolds number solution. The quantities  $\max_x\{b_n\}$  and  $\max_x\{a_n\}$  as a function of  $n$  are shown, in the left and in the right panel, respectively.

where  $\alpha_0$  is the amplitude of the  $\alpha$ -effect and  $x_\alpha$ ,  $x_\beta$  and  $d$  define the location and the thickness of the turbulent layer, respectively. Differently from the overshoot dynamo  $\alpha_0$  is *not* assumed to change its sign in the bulk of the convection zone or in the overshoot layer. In Fig. 3 the eddy diffusivity profile and the  $\alpha$  profile are shown for  $x_\alpha = 0.9$ ,  $x_\beta = 1$  and  $d = 0.05$  which correspond to an  $\alpha$ -effect located at the top of the convection zone.

### 3. Mathematics and numerics

In order to investigate the properties of the solar dynamo with such a low eddy diffusivity we solve the linear dynamo Eq. (3) with a finite-difference scheme for the radial dependence and a polynomial expansion for the angular dependence. In particu-

lar, we have used the following expansions for the field:

$$\hat{A}(x, \theta) = e^{\lambda t} \sum_n a_n(x) P_n^{(1)}(\cos \theta), \quad (10)$$

$$\hat{B}(x, \theta) = e^{\lambda t} \sum_m b_m(x) P_m^{(1)}(\cos \theta), \quad (11)$$

where  $\lambda$  is the (complex) eigenvalue,  $n = 1, 3, 5, \dots$  and  $m = 2, 4, 6, \dots$  for antisymmetric modes, and  $n \leftrightarrow m$  for symmetric modes. Vacuum boundary conditions at the surface are then translated into

$$\frac{da_n}{dx} + (n+1) a_n = b_m = 0. \quad (12)$$

In the interior at  $x = x_i = 0.6$  we have instead set

$$x \frac{db_m}{dx} + b_m = a_n = 0, \quad (13)$$

which imply perfect conductor boundary conditions for the field.

By substituting (10) and (11) in (3) one obtains a set of infinite o.d.e. that can be conveniently truncated in  $n$  when the desired accuracy is achieved. The system is in fact solved by means of a second order accuracy finite difference scheme and the basic computational task is thus to numerically compute eigenvalues and eigenvectors of a block-band diagonal real matrix of dimension  $M \times n$ ,  $M$  being the number of mesh points and  $n$  the number of harmonics. This basic algorithm is embedded in a bisection procedure in order to determine the critical  $\alpha$ -value needed to find a purely oscillatory solution. This value is accepted when the dimensionless quantity  $\Re(\lambda)R_\odot^2/\eta_T$  is no greater than  $10^{-3}$ .

We have first tested the accuracy of our code in simple cases where the eigenvalues and eigenfunctions are known (decay modes with  $\alpha = 0$  and simple analytic solutions with constant  $\alpha$ ). Then, we have checked most of the solutions discussed in the literature (no flow) and we found good agreement. In fact we have rapid convergence in  $n$  for simple (no-flow)  $\alpha\Omega$ -dynamo, and we could confirm most of the findings by Steenbeck & Krause (1969) and Roberts (1972). When the flow is present, the number of harmonics needed in order to get convergence generally increases with the Reynolds number and we decided to truncate the series (12-13) when the maximum value over  $x$  of the  $n$ -th harmonic drops by roughly three orders of magnitude, as shown in Fig. 4.

### 4. Numerical results

We performed an extensive numerical exploration of the parameter space, allowing simultaneous variations of  $x_\alpha$ ,  $\eta_c/\eta_t$ ,  $u_m$  and angular dependence of the  $\alpha$ -effect, considering both  $\cos \theta$  and  $\cos \theta \sin^2 \theta$  functions in (9). In all models discussed in the following the rotation law is given by helioseismology and the eddy diffusivity is fixed to be  $\eta_T = 10^{11} \text{ cm}^2/\text{s}$ . The drift amplitude is considered as a free parameter of the order of 1 m/s up to 10 m/s. In some cases we have investigated the field configuration for very strong flow up to 20 m/s.

#### 4.1. Alpha-effect in the entire convection zone

We start with a model where the (positive)  $\alpha$ -effect exists through the whole convection zone ( $x_\alpha = 0.7$ ,  $x_\beta = 1$ ,  $d = 0.05$ ). In Table 1 the results are given. Suffix A denotes the (dipolar) solutions with antisymmetry with respect to the equator and suffix S denotes the (quadrupolar) solutions with symmetry with respect to the equator. The drift amplitude varies between 2 cm/s and 10 cm/s. For small flow the dipole-solution occurs with the lowest  $\alpha$ -effect amplitude, but for higher values of the flow the quadrupole solution is more easily excited. The oscillation period of the linear dynamo is also given: for high value of the flow quadrupole solutions have cycles which are longer than the corresponding dipole ones. This is a property that we have verified for all cases in the rest of paper, namely that in the high Reynolds number regime, lowest  $\alpha$ -value solutions have longer periods than the corresponding opposite parity solutions.

It should also be noticed that, with the small value of eddy diffusivity we have chosen, the cycle period becomes rather long compared with the 22-years of the Sun. As we know from the theory of the overshoot dynamo, the inclusion of the nonlinear feedback of the magnetic field (via  $\alpha$ -quenching) reduces the periods to more realistic values (Rüdiger & Brandenburg 1995). What we are interested in, is mainly the influence of the  $\alpha$ -effect profile and the drift amplitude on the resulting parity of the solutions. Figures 5 and 6 show the magnetic topology of the dynamo with 3 m/s drift amplitude. We find (for the lowest eigenvalue) a solution with antisymmetry with respect to the equator. The toroidal field belts are concentrated at the bottom of the convection zone, and the poloidal field exhibits, close to the surface, a rather small-scaled structure (Fig. 5). The toroidal field belts migrates equatorwards but, however, the maximal field strength occurs in the polar region.

**Table 1.** Critical  $\alpha$ -values (cm/s) and periods  $P$  (yrs) for models with  $\alpha$ -effect in the entire convection zone. Bold is used when the dipolar solution has the smallest  $\alpha$ -value. The quadrupolar symmetry is denoted by “S” (“symmetric”) and the dipolar parity symmetry by “A” (antisymmetric).

$u_m$	$\alpha_A$	$P_A$	$\alpha_S$	$P_S$
2.0	<b>0.90</b>	$\infty$	1.28	131
3.0	1.83	82	1.70	83
6.0	2.46	51	2.17	54
10.0	3.93	37	3.45	41

#### 4.2. Alpha-effect at the top

We now consider models where the  $\alpha$ -effect is located at the top of the convection zone as discussed in the models of Küker et al. (2001). The results of the simulations confirm the basic features of the advection-dominated dynamo, namely that, for a flow of few m/s and a low diffusivity, the butterfly diagram

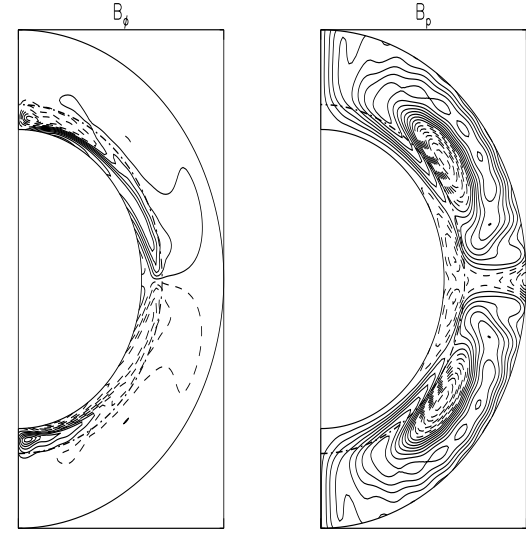


**Fig. 5.** Alpha-effect in the entire convection zone: Toroidal (left) and poloidal (right) antisymmetric (dipolar) field configuration for  $u_m = 6$  m/s at  $t = 0$ . The  $\alpha$ -effect is located between  $x_\alpha = 0.7$  and  $x_\beta = 1$ . The solution is plotted as  $B_\phi$ -isocontours and poloidal magnetic field lines. Solid contours (field lines) correspond to positive toroidal fields (pointing into the plane of the paper) and dashed contours to negative toroidal field (pointing out of the paper) .

shows the correct equatorward migration of the toroidal field, and the phase relation of the magnetic fields is mostly negative as shown in Fig. 7. We found that, as far as the parity model selection is concerned, variations of the ratio  $\eta_c/\eta_t$  are not particularly significant, while a functional dependence of the type  $\cos \theta \sin^2 \theta$  for the  $\alpha$ -effect disfavours the appearance of dipolar field configurations. We have then considered variations of the thickness of the  $\alpha$ -layer. The results of this investigation are summarized in Fig. 8 and in Tables 2 and 3. For a slow

**Table 2.** Alpha-effect at the top (thick layer): Critical  $\alpha$ -values (cm/s) and periods (yrs) for various values of the flow (m/s), for both antisymmetric (A) and symmetric field (S) configurations with  $x_\alpha = 0.8$ ,  $x_\beta = 1$ ,  $\eta_c/\eta_t = 0.02$ .

$u_m$	$\alpha_A$	$P_A$	$\alpha_S$	$P_S$
1.0	0.96	$\infty$	0.79	$\infty$
1.5	1.56	$\infty$	1.28	$\infty$
2.0	<b>1.86</b>	222	2.02	$\infty$
2.5	2.22	160	1.83	162
3.0	2.58	130	1.99	134
3.5	2.95	112	2.21	119
5.0	4.03	83	2.97	100
10	7.30	51	5.67	59
20	12.1	37	9.86	42

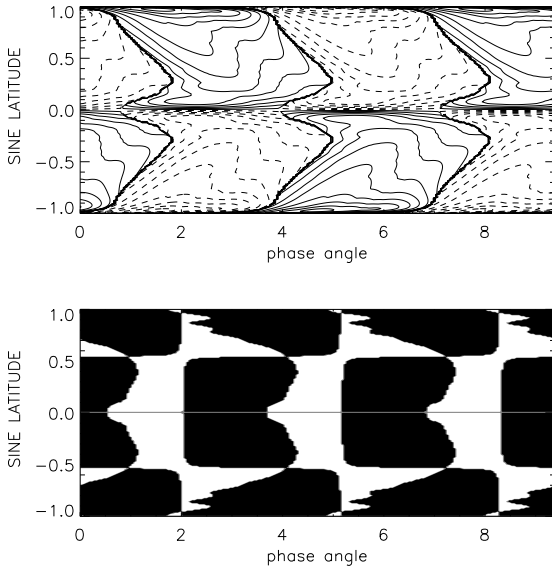


**Fig. 6.** Alpha-effect in the entire convection zone: Butterfly diagram (top) and field phase relation (bottom) of a dynamo with critical turbulence  $\alpha_0 = 2.46$  cm/s,  $u_m = 6$  m/s. Black colors means negative  $B_r B_\phi$ . The  $\alpha$ -effect is located between  $x = 0.7$  and  $x = 1$ .

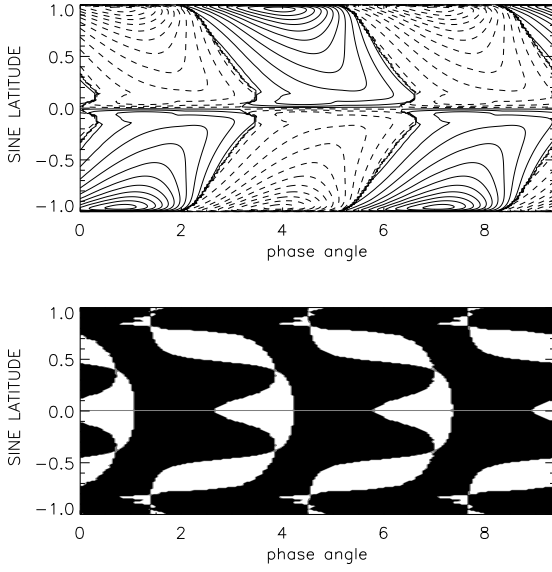


**Fig. 7.** Alpha-effect at the top: Butterfly diagram (top) and field phase relation (bottom) of a dynamo with critical turbulence  $\alpha_0 = 10.8$  cm/s,  $u_m = 10$  m/s,  $x_\alpha = 0.9$ ,  $x_\beta = 1$ . Black colors means negative  $B_r B_\phi$ .

flow, both quadrupoles and dipoles have similar excitation conditions. For intermediate values of the flow amplitude, it is possible to have a different dynamo mechanism working and the solutions are stationary. In particular, as it is shown in Tables 2

**Table 3.** Alpha-effect at the top (thin layer): Critical  $\alpha$ -values (cm/s) and periods (yrs) for various values of the flow (m/s), for both antisymmetric and symmetric field configurations with  $x_\alpha = 0.9$ ,  $x_\beta = 1$ , and  $\eta_c/\eta_t = 0.02$ . The dipole solutions with lowest critical  $\alpha$ -value are shown in bold.

$u_m$	$\alpha_A$	$P_A$	$\alpha_S$	$P_S$
1.0	4.44	$\infty$	9.05	312
1.5	<b>5.63</b>	$\infty$	4.03	$\infty$
2.0	7.11	$\infty$	5.11	$\infty$
2.5	8.79	$\infty$	6.41	$\infty$
3.0	<b>7.24</b>	253	7.93	$\infty$
3.5	<b>7.63</b>	226	9.61	$\infty$
5.0	9.88	176	6.59	137
10	19.1	90	11.4	88
24	39.1	41	28.8	44

and 3, dipole solutions may have a smaller critical  $\alpha_0$ -value in this case.

In the high-Reynolds numbers regime, quadrupole fields are more easily excited and the cycle periods drastically reduce. We confirm the findings by Dikpati & Charbonneau (1999) as far as the global structure of the field and the parity problem (Dikpati & Gilman 2001) is concerned. For a flow of 10 m/s the field geometry is shown in Fig. 9 and the mode with the lowest eigenvalue is a quadrupole.

#### 4.3. Alpha-effect at the bottom

This picture drastically changes if the  $\alpha$ -effect operates at the bottom of the convection zone. We have considered a thin and a thick  $\alpha$ -layer. In the first class of models  $x_\alpha = 0.7$  and  $x_\beta = 0.8$  while in a second class  $x_\alpha = 0.7$  and  $x_\beta = 0.9$ .

Figures 10 and 11 show an example of a model of the first class. Again, the toroidal field is concentrated at the bottom of the convection zone, where, however, the highest field amplitudes occur in the polar regions. The diagram for  $B_r \cdot B_\phi$  shows the dominance of the negative sign.

In Fig. 12 parity and cycle periods of the solution for the model with a thin  $\alpha$ -layer at the bottom of the convection zone are given. The solution with the dipolar symmetry has the lowest  $\alpha$ -value and is the stable one. There is no heavy parity problem if the  $\alpha$ -layer is located at the base of the convection zone (see Dikpati & Gilman 2001). However, we can also notice from Fig. 12 (lower panel) that in this case the oscillation period of the dipoles is longer than for the quadrupoles, while, for slow flows, the cyclic behaviour of the dynamo solution disappears, so that only meridional flows with amplitudes exceeding 3 m/s are here relevant. In this case the dipole solutions do not match the 22-year cycle period of the Sun (although the quadrupoles do). The overall result is that the dipolar solutions are always more easily excited and also the butterfly diagram shows the correct characteristics.

In the second class of models the dynamo mechanism was of the same type, as we could infer from the field configuration

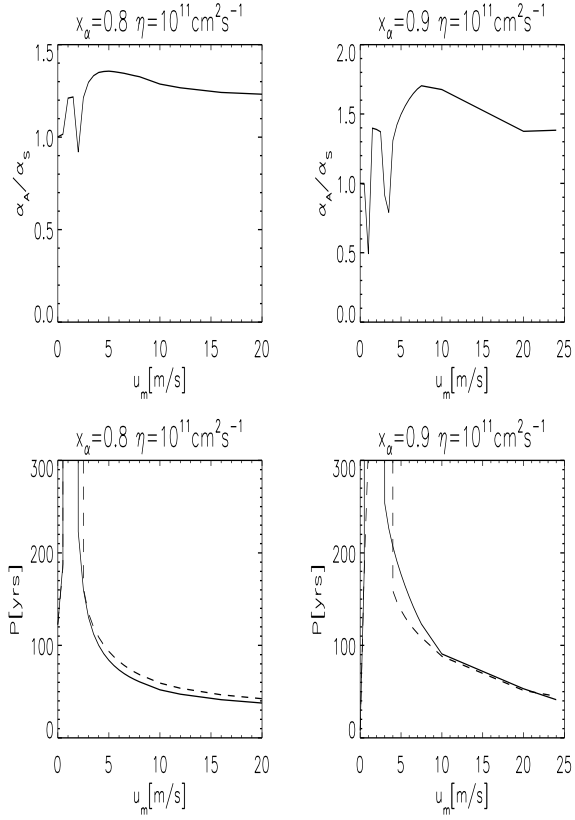


**Fig. 8.** Alpha-effect at the top: The ratio  $\alpha_A/\alpha_S$  of the critical  $\alpha$ -numbers for antisymmetric and symmetric field configurations is shown (as in Fig. 1) as a function of the flow speed  $u_m$  in the panels above. The period (continuous line for the anti-symmetric modes, dashed line for symmetric modes) is shown in panels below. The presence of vertical lines indicates that the solution is stationary

and from the butterfly diagram (not shown). However in this case the quadrupolar solution was always the most easily excited. From these results we can deduce that the region where the  $\alpha$ -effect produces more easily dipolar field configuration, in the advection-dominated regime, is below  $x \approx 0.8$ .

#### 4.4. Very thin $\alpha$ -layer

In this case we have set  $x_\alpha = 0.7$ ,  $x_\beta = 0.75$ ,  $d = 0.02$  and the relevant results are summarized in Table 4, where it is possible to notice that for a thin  $\alpha$ -layer at the bottom, the dipolar field configuration is the most easily excited. We noticed that if no flow is present there is no migration towards lower latitudes of the magnetic field. However for moderate flow the maximum of the toroidal field is in the equatorial region, as is possible to see in Fig. 13 and Fig. 14. For stronger flow the period matches the observed one as shown in Table 4. In this case dipolar and quadrupolar solutions have greater dynamo numbers than in the slow flow case, but the dipolar field configuration is always the favoured one. The field configuration and the butterfly diagram are shown in Fig. 15 and 16. Conversely, a very thin  $\alpha$ -layer lo-

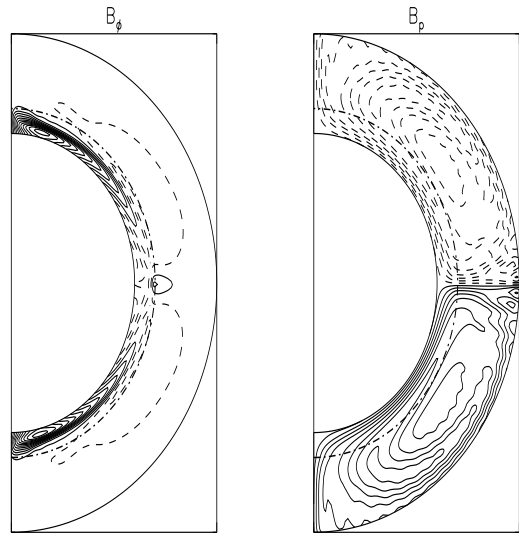


**Fig. 9.** Alpha-effect at the top: Toroidal (left) and poloidal (right) symmetric (quadrupolar) field configuration for  $\alpha_0 = 8.95 \text{ cm/s}$ ,  $x_\alpha = 0.9$ ,  $x_\beta = 1$ ,  $d = 0.02$ ,  $\eta_c/\eta_t = 0.1$ ,  $u_m = 10 \text{ m/s}$  at  $t = 0$

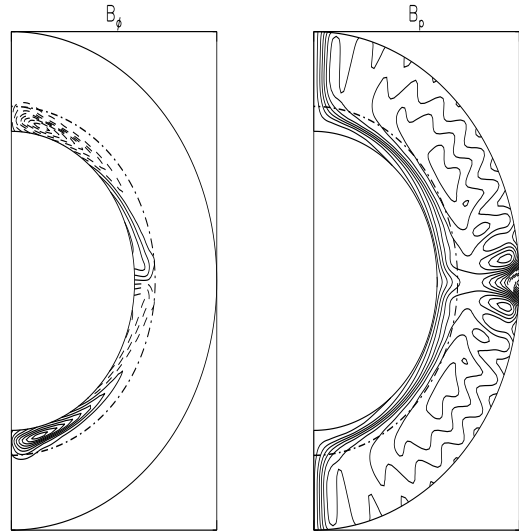


**Fig. 10.** Alpha-effect at the bottom: Toroidal (left) and poloidal (right) antisymmetric (dipolar) field configuration for  $\alpha = 0.95 \text{ cm/s}$ ,  $u_m = 6 \text{ m/s}$  at  $t = 0$ . The  $\alpha$ -effect is located between  $x_\alpha = 0.7$  and  $x_\beta = 0.8$ .

cated at the top of the convection zone produces a much larger dynamo number and the solution is always symmetric as shown in Table 4.

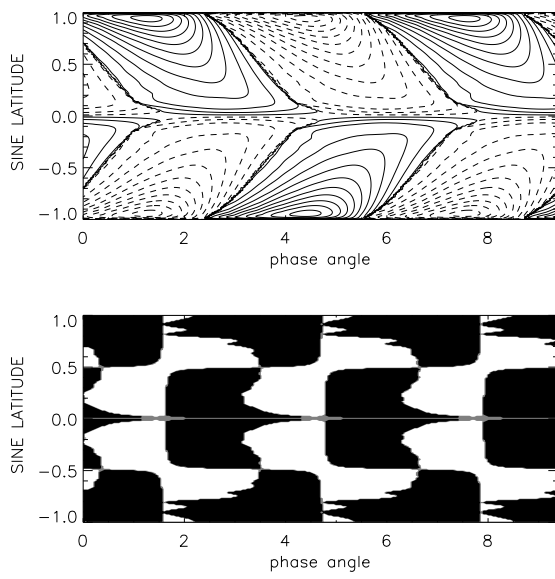


**Fig. 11.** The same as in Fig. 7 but for the model presented in Fig. 10. The cycle period is 120 years.

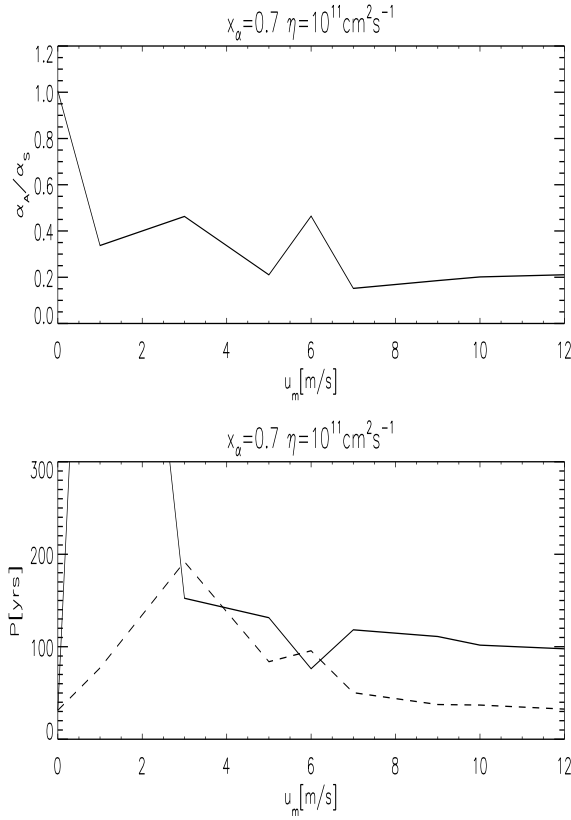


**Fig. 12.** The same as in Fig. 8 but for models with the  $\alpha$ -effect located at the bottom of the convection with  $x_\alpha = 0.7$  and  $x_\beta = 0.8$ . Note the clear dominance of dipolar solutions indicated by their much smaller dynamo numbers.

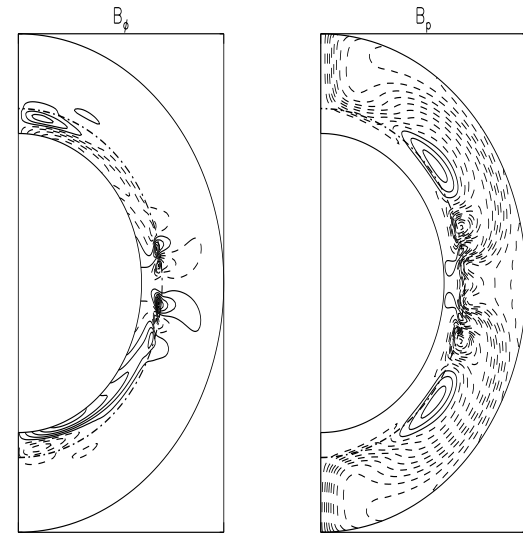


**Fig. 13.** Thin Alpha-effect at the bottom: Toroidal (left) and poloidal (right) antisymmetric (dipolar) field configuration for  $\alpha = 4.36 \text{ cm/s}$ ,  $u_m = 3 \text{ m/s}$  at  $t = 0$  and  $x_\alpha = 0.7$ ,  $x_\beta = 0.75$ .

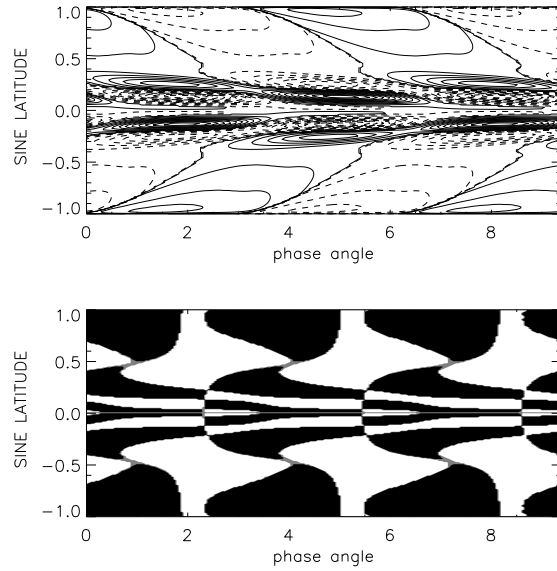


**Fig. 14.** The same as in Fig. 7 but for the model presented in Fig. 13. The cycle period is 74 years.

## 5. Conclusions

A kinematic solar dynamo has been studied with the flow pattern taken from observations (rotation law) and theory (meridional flow). An eddy diffusivity of  $10^{11} \text{ cm}^2/\text{s}$  provides us with a value consistent with the sunspot decay. With such a small value the magnetic Reynolds number for a meridional flow of (say)  $10 \text{ m/s}$  reaches values of order of  $10^3$ , so that the dynamo can really be called advection-dominated. The meridional flow

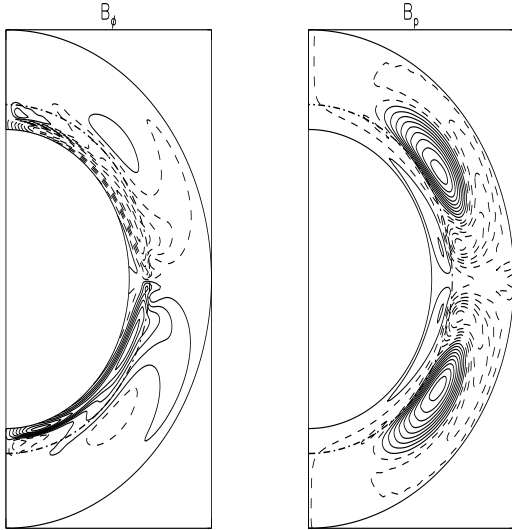


**Fig. 15.** Alpha-effect at the bottom for a very thin layer: toroidal (left) and poloidal (right) antisymmetric (dipolar) field configuration for  $\alpha = 16.61$  cm/s,  $u_m = 12$  m/s at  $t = 0$  and  $x_\alpha = 0.7$ ,  $x_\beta = 0.75$ .

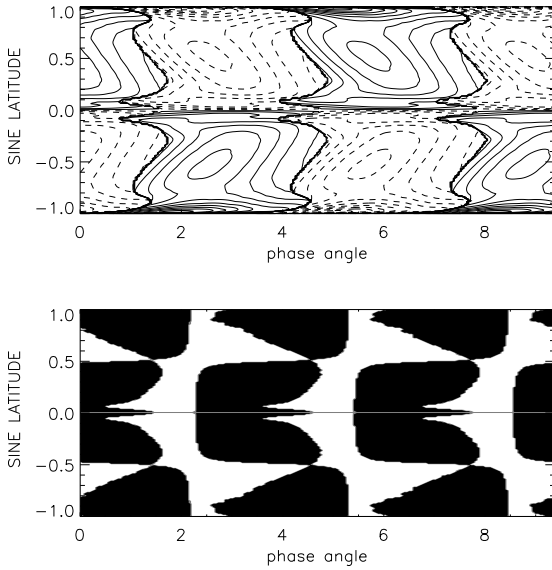


**Fig. 16.** The same as in Fig. 7 but for the model presented in Fig. 15. The cycle period is 23 years.

at the bottom of the convection zone is supposed to drift equatorwards (and polewards at its top) as can be deduced by the mean-field theory of the differential rotation in an outer convection zone (Kitchatinov & Rüdiger 1999; Miesch et al. 2000). When this happens, the meridional flow advects the field equatorwards producing a butterfly diagram of the observed type, which would not occur with i) a positive  $\alpha$ -effect (in the northern hemisphere), ii) the standard rotation law known from helio-

**Table 4.** Critical  $\alpha$ -values (cm/s) and periods (yrs) for a very thin  $\alpha$ -layer located between  $x_\alpha = 0.7$  and  $x_\beta = 0.75$  for various values of the flow (m/s), for both antisymmetric and symmetric field configurations. In the last line the same  $\alpha$ -layer is located between  $x_\alpha = 0.95$  and  $x_\beta = 1$  and the solution is clearly of the symmetric type. Also notice the much larger dynamo number in this latter case.

$u_m$	$\alpha_A$	$P_A$	$\alpha_S$	$P_S$
1	<b>0.43</b>	$\infty$	1.14	90.8
2	<b>1.37</b>	$\infty$	1.83	$\infty$
3	<b>4.36</b>	74	4.94	64
5	<b>7.53</b>	38	8.46	35
7	<b>9.22</b>	34	9.65	33
12	<b>16.61</b>	23	16.77	23
2	87	$\infty$	50	283
20	43	94	40	68

seismology and iii) no meridional flow (Choudhuri et al. 1995; Dikpati & Charbonneau 1999; Küker et al. 2001). As Dikpati & Gilman (2001) have stressed, these models may encounter a problem with the parity of the solution since for most of the models the quadrupolar solution is the stable one. We have used this striking fact to discuss the effect of the radial distribution of the  $\alpha$ -effect on the parity model selection. Our conclusion is that a thin  $\alpha$ -layer located below  $r/R_\odot \approx 0.8$  selects models with correct parity property, butterfly diagram phase relation and cycle periods close to the observed one. This confirms the findings of Dikpati & Gilman (2001), providing further evidence for a tachocline  $\alpha$ -effect as a promising candidate for understanding the dynamo mechanism operating in the Sun.

## References

Abramenko, V.I., Wang, T., & Yurchishin, V.B. 1996, *Sol. Phys.*, 168, 75  
 Bao, S., & Zhang, H. 1998, *ApJ*, 496, L43  
 Brandenburg, A. 1999, Helicity in Large-scale Dynamo Simulations, in *Magnetic Helicity in Space and Laboratory Plasmas*, ed. M.R. Brown, R.C. Canfield, & A.A. Pevtsov (American Geophysical Union, Washington), 65  
 Choudhuri, A.R., Schüssler, M., & Dikpati, M. 1995, *A&A*, 303, L29  
 Dikpati, M., & Charbonneau, P. 1999, *ApJ*, 518, 508  
 Dikpati, M., & Gilman, P.A. 2001, *ApJ*, 559, 428  
 Dikpati, M., & Gilman, P.A. 2001, Symmetry Selection in Solar Cycle Dynamo Models, in *Magnetic Fields across the Hertzsprung-Russell Diagram*, ed. G. Mathys, S.K. Solanki, & D.T. Wickramasinghe, *ASP Conf. Ser.*, 248 (Sheridan Books, Chelsea), 125  
 Kitchatinov, L.L., & Rüdiger, G. 1992, *A&A* 260, 494  
 Kitchatinov, L.L., & Rüdiger, G. 1999, *A&A*, 344, 911  
 Köhler, H. 1973, *A&A*, 18, 453  
 Küker, M., Rüdiger, G., & Schultz, M. 2001, *A&A*, 374, 301  
 Markiel, J.A., & Thomas, J.H. 1999, *ApJ*, 523, 827  
 Miesch, M.S., Elliot, J.R., Toomre, J., Clune, T.L., Glatzmaier, G.A., & Gilman, P.A. 2000, *ApJ*, 532, 593  
 Moss, D. 1999, *MNRAS*, 306, 300  
 Moss, D., & Brooke, J. 2000, *MNRAS*, 315, 521  
 Pevtsov, A.A., Canfield, R.C., & Metcalf, T.R. 1995, *ApJ*, 440, L109

Rädler, K.-H., & Seehafer, N. 1990, Relations between Helicities in Mean-field Dynamo Models, in Topological Fluid Mechanics, ed. H.K. Moffatt, & A. Tsinober (Cambridge University Press, Cambridge), 157

Roberts, P. 1972, Phil. Trans. Roy. Soc. A, 272, 663

Roberts, P., & Stix, M. 1972, A&A, 18, 453

Rüdiger, G. 1989, Differential Rotation and Stellar Convection: Sun and Solar-type stars. (Gordon & Breach Science Publishers, New York)

Rüdiger, G., & Brandenburg, A. 1995, A&A, 296, 557

Rüdiger, G., Pipin, V.V., & Belvedere, G. 2001, Sol. Phys., 198, 241

Seehafer, N. 1990, Sol. Phys., 125, 219

Steenbeck, M., & Krause, F. 1969, Astron. Nachr., 291, 49

Wang, Y.-M., Sheeley, N.R., Jr., & Nash, A.G. 1991, ApJ, 383, 431